A biomimetic approach to inverse kinematics for a redundant robot arm

Citation: Artemiadis, Panagiotis K., Pantelis T. Katsiaris, and Kostas J. Kyriakopoulos. "A Biomimetic Approach to Inverse Kinematics for a Redundant Robot Arm." Autonomous Robots 29.3-4 (2010) : 293-308.

As Published: http://dx.doi.org/10.1007/s10514-010-9196-x

Publisher: Springer Science + Business Media B.V.

Persistent URL: http://hdl.handle.net/1721.1/65149

Version: Author's final manuscript: final author's manuscript post peer review, without publisher's formatting or copy editing

Noname manuscript No.
(will be inserted by the editor)

A biomimetic approach to inverse kinematics for a redundant robot arm

Panagiotis K. Artemiadis · Pantelis T. Katsiaris · Kostas J. Kyriakopoulos

Received: date / Accepted: date

Abstract Redundant robots have received increased attention during the last decades, since they provide solutions to problems investigated for years in the robotic community, e.g. task-space tracking, obstacle avoidance etc. However, robot redundancy may arise problems of kinematic control, since robot joint motion is not uniquely determined. In this paper, a biomimetic approach is proposed for solving the problem of redundancy resolution. First, the kinematics of the human upper limb while performing random arm motion are investigated and modeled. The dependencies among the human joint angles are described using a Bayesian network. Then, an objective function, built using this model, is used in a closed-loop inverse kinematic algorithm for a redundant robot arm. Using this algorithm, the robot arm end-effector can be positioned in the three dimensional (3D) space using human-like joint configurations. Through real experiments using an anthropomorphic robot arm, it is proved that the proposed algorithm is computationally fast, while it results to human-like configurations compared to previously proposed inverse kinematics algorithms. The latter makes the proposed algorithm a strong candidate for applications where anthropomorphism is required, e.g. in humanoids or generally in cases where robotic arms interact with humans.

Keywords Inverse kinematics · Biomimetics · Redundant Robots · Graphical Models · Anthropomorphic Motion

1 Introduction

Robot configuration plays a very significant role in a growing number of robot applications. In certain complex industrial tasks, stable, fast and accurate robot positioning is required, while in a number of nonindustrial tasks (e.g. domestic robotics, robotic-assisted surgery etc) dexterity and intelligent positioning is required to avoid obstacles [1], joint limits [2] or singular configurations [3]. For all those reasons, redundant robots have received increased attention during the last decades, along with their associated problem of complex kinematics. Since their joint configuration is not determined uniquely, a set of kinematic and dynamic criteria have been introduced to achieve a unique solution [4]. During the last decade though, the robots are getting closer to humans, introducing thus the need for anthropomorphic motion to allow improved interaction. Towards this goal, the multijoint coordination of the human arm should be analyzed and modeled. If joint angles dependencies are modeled, then incorporating those synergies in the inverse kinematics algorithms results to a biomimetic approach of the kinematic control of redundant robot arms.

Panagiotis K. Artemiadis
Department of Mechanical Engineering,
Massachusetts Institute of Technology (MIT),
Cambridge, MA, 02139 USA
Tel.: +1 617-253-8114
E-mail: partem@mit.edu

Pantelis T. Katsiaris
Control Systems Lab, School of Mechanical Eng.,
National Technical University of Athens,
9 Heroon Polytechniou Str, Athens, 157 80, Greece
Tel.: +30 210-772-4012
E-mail: katsiaris@gmail.com

Kostas J. Kyriakopoulos
Control Systems Lab, School of Mechanical Eng.,
National Technical University of Athens,
9 Heroon Polytechniou Str, Athens, 157 80, Greece
Tel.: +30 210-772-3595
E-mail: kkyria@mail.ntua.gr

The investigation of human arm motion, in order to infer laws for biomimetic trajectory planning and robot inverse kinematics, has been reported in the past [5]. Especially for everyday life tasks (e.g. drawing, handwriting), approaches of mimicking the human arm movements have been proposed [6]. Some studies have been also done in order to generate human-like motion by imitating human arm motion as closely as possible. In most of these studies, the human motion is measured using a motion capture system and then converted to motion for a humanoid robot arm [7]. In [8] a method is proposed to convert the captured marker data of human arm motions to robot motion using an optimization scheme. The position and orientation of the human hand, along with the orientation of the upper arm, were imitated by a humanoid robot arm. However, this method was not able to generate human like motions, given a desired three dimensional (3D) position for the robot end-effector. Similarly, most of the previous works on biomimetic motion generation for robots are based on minimizing posture difference between the robot and the human arm, using a specific recorded data set [7]. Therefore, the robot configurations are exclusively based on the recorded data set. In this way, the method can not generate new human-like motion, which is quite important for the kinematic control of anthropomorphic robot arms and humanoids, where the range of possible configurations should not be limited to the ones recorded from humans.

Cost functions have been also proposed to model motion principles of human arm movements [9]. However these functions are quite complex to be used for the inverse kinematics of robots, while they are usually addressing not only the kinematic, but also to the dynamic level. Other kinematic or dynamic criteria were proposed in the past [20], [21], however they were not addressing arm motion in the 3D space. Moreover, Hidden Markov Models (HMM) were used in the past for modeling arm motion towards robot imitation [22], [23], [26], [28], however most of the works are based on cost functions and optimization techniques that drive the robots based on a finite recorded set, while the models are not able to generalize. A set of nonlinear dynamical systems and discrete control policies were introduced in [24], a finite set of primitives were used to control a humanoid in [25], while similar control strategies based on primitives were used in [29]. Motion graphs were used in [27], however the probabilistic characteristics were used to connect certain patterns of motion with an existing database of recorded arm movements. Finally, a partitioning of the human-like motion generation problem in robots has been proposed in the past [10]. The upper arm joints values are first calculated for positioning the robot elbow, and then using that, the rest of the joints are evaluated. Such an approach though can not be easily applied to robots having a kinematic structure different from that of the human upper limb.

In this paper a biomimetic approach for solving the inverse kinematic problem of redundant robot arms is proposed. The idea of using the analysis of the human arm multijoint coordination, in order to synthesize motion patterns for robot arms, is utilized. Human arm motion during everyday life tasks, like reaching objects or wiping a surface, is recorded and analyzed. The motion analyzed here excludes the wrist motion, therefore accounts for 5 degrees of freedom (shoulder and elbow), which suffice for arm tasks in the 3D space. A Bayesian Network is used for the probabilistic description of the human arm multijoint coordination. Then an objective function is defined based on the interjoint dependency described by the probabilistic model. This function is incorporated into a closed-loop inverse kinematics algorithm for a redundant robot arm. Using the proposed method, an anthropomorphic redundant robot arm is kinematically controlled in end-effector positioning tasks. The computational time of the inverse kinematics is negligible while the resulting robot arm configuration is anthropomorphic, as assessed through the comparison of joint angle profiles with the previously recorded human arm data. Moreover, the proposed model can generate new human-like robot arm motions, that are not limited to the repertoire of motions initially recorded from the human arm.

One of the main differences that this work has, compared to previous ones, is that it doesn't depend on robots mimicking a pre-defined set of human arm motion. Furthermore, the work is not based on any algorithm that tries to minimize the differences between the robot motion and the pre-recorded human motion. In contrary to the previous works, the method proposed in this paper tries to mathematically model the anthropomorphic characteristics of human arm motion. Based on the resulted model, a closed-loop inverse kinematic method is used in order to create anthropomorphic configurations for the robot arm, without directly mimicking pre-recorded human arm motions. Moreover, through the model trained, new[1] anthropomorphic robot arm motions are generated, proving not only the ability of the proposed method to effectively describe anthropomorphic arm motions but also the generalization properties of the proposed model.

The rest of the paper is organized as follows: the proposed methodology is presented in Section 2. The

[1] New arm motions are considered those that are different from a continuous finite set recorded during model training.

experimental procedure assessing the method efficiency is reported in Section 3, while Section 4 concludes the paper.

2 Methodology

2.1 Human Arm Motion Analysis

There is no doubt that the kinematic structure of the human upper extremity is quite efficient, while very complex. Narrowing our interest down to the upper limb and not considering finger motion, the kinematics of the arm can be modeled with 7 degrees of freedom. In this study, we focused on the principal joints of the upper limb, i.e. the shoulder and the elbow. The wrist motion was not included in the analysis for simplicity. The proposed method was used for the control of an anthropomorphic robot arm, equipped with rotational joints that mimic the degrees of freedom of the human arm, as shown in Fig. 1. Therefore, 5 degrees of freedom were analyzed; shoulder abduction-adduction, shoulder flexion extension, shoulder external-internal rotation, elbow flexion-extension and forearm pronation-supination, which can be simulated by 5 corresponding joint angles, i.e. q_1, q_2, q_3, q_4, q_5 for the human arm and q_{1R}, q_{2R}, q_{3R}, q_{4R}, q_{5R} for the robot arm respectively, as shown in Fig. 1. A training session was conducted, during which motion data from the human arm performing random motions in the 3D space were recorded. Motion data were then used for building a model describing human arm multi-joint dependencies, that was used in the proposed approach for the robot inverse kinematics. Four subjects at the age range of 25-29 participated at the experiments.

In order to record the motion of the upper limb and then extract the joint angles of the 5 modeled degrees of freedom, a magnetic position tracking system was used. The system was equipped with two position trackers and a reference system, with respect to which, the 3D position and orientation of the trackers were provided. In order to compute the 5 joint angles, one position tracker was placed at the user's elbow joint while the other one at the wrist joint. The reference system was placed on a solid surface above the user's shoulder. The surface was properly aligned with respect to the subject sagittal and coronal plane, so the planes of the tracker reference system were aligned to the corresponding planes of the user. Moreover the users had their back attached to a chair's back by means of elastic straps, in order to prevent motion of the torso while moving the arm. The proper computation on the tracker measurements were done in order to "virtually" transfer the center of the tracker reference system as close as possible to the center of the shoulder joint. The setup is shown in Fig. 1, where the "virtual" tracker base reference system is shown on the user's shoulder. The kinematic analysis is summarized in the following paragraph, while for more details the reader should refer to Appendix A.

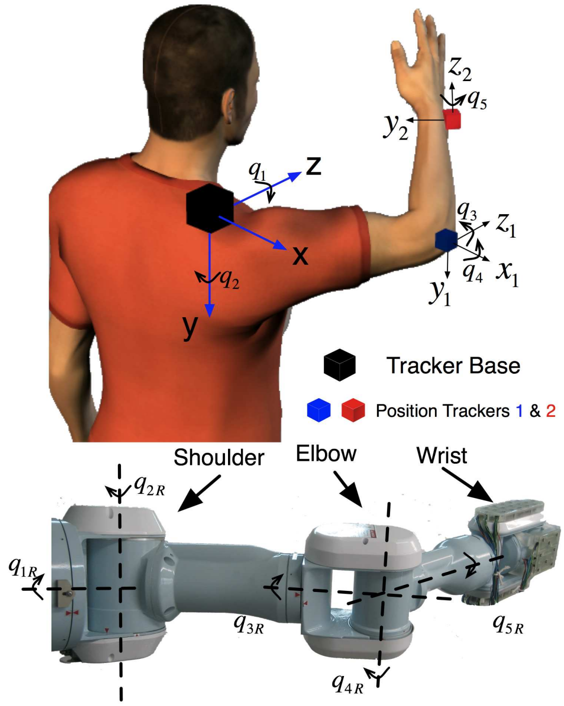

Fig. 1 Human and robot joint angles. The equivalence of the human and robot degrees of freedom is shown. The two position trackers are placed on the user elbow and wrist joint, while the tracker reference system is placed on the user's shoulder.

Let $\mathbf{T_1} = \left[x_1 \; y_1 \; z_1\right]^T$, $\mathbf{T_2} = \left[x_2 \; y_2 \; z_2\right]^T$ denote the position of the trackers with respect to the tracker reference system. Measurements of $\mathbf{T_1}$, $\mathbf{T_2}$ were provided by the position tracking system at the frequency of 60 Hz. By solving the inverse kinematic equations the human joint angles were given by:

$$\begin{aligned}
q_1 &= \arctan 2\left(\pm y_1, x_1\right) \\
q_2 &= \arctan 2\left(\pm\sqrt{x_1^2 + y_1^2}, z_1\right) \\
q_3 &= \arctan 2\left(\pm B_3, B_1\right) \\
q_4 &= \arctan 2\left(\pm\sqrt{B_1^2 + B_3^2}, B_2 - L_1\right) \\
q_5 &= \arctan 2\left(\mathrm{M}, \Lambda\right) + \arctan 2\left(1 \pm \sqrt{\tfrac{\mathrm{K}^2}{\mathrm{M}^2+\Lambda^2}}, \tfrac{\mathrm{K}}{\sqrt{\mathrm{M}^2+\Lambda^2}}\right)
\end{aligned} \tag{1}$$

where

$$\begin{aligned}
B_1 &= x_2\cos\left(q_1\right)\cos\left(q_2\right) + y_2\sin\left(q_1\right)\cos\left(q_2\right) - z_2\sin\left(q_2\right) \\
B_2 &= -x_2\cos\left(q_1\right)\sin\left(q_2\right) - y_2\sin\left(q_1\right)\sin\left(q_2\right) - z_2\cos\left(q_2\right) \\
B_3 &= -x_2\sin\left(q_1\right) + y_2\cos\left(q_1\right) \\
\mathrm{K} &= \tan\left(\phi\right)\left(\cos\left(q_2\right)\cos\left(q_4\right) - \cos\left(q_3\right)\sin\left(q_2\right)\sin\left(q_4\right)\right) \\
\Lambda &= \sin\left(q_2\right)\sin\left(q_3\right) \\
\mathrm{M} &= \cos\left(q_3\right)\cos\left(q_4\right)\sin\left(q_2\right) + \cos\left(q_2\right)\sin\left(q_4\right)
\end{aligned} \tag{2}$$

where ϕ was the roll angle measured from the position tracker 2 and L_1 was the length of the upper arm. The length of the upper arm was computed from the distance of the first position tracker from the base reference system, i.e. $L_1 = \|\mathbf{T_1}\| = \sqrt{x_1^2 + y_1^2 + z_1^2}$. Likewise, the length of the forearm L_2 was computed from the distance between the two position trackers, i.e. $L_2 = \sqrt{(x_2 - x_1)^2 + (y_2 - y_1)^2 + (z_2 - z_1)^2}$.

Since the position trackers were placed on the skin and not in the center of the modeled joints (which would be impractical), the lengths L_1, L_2 could slightly vary as the user moved the arm. A variance of approximately $0.01m$ was observed for the lengths L_1, L_2. Moreover, for all subjects, the measured lengths' values were very close[2] to the actual anatomical ones. However, very accurate measurements for human joint angles is not a critical factor for the proposed method. The paper proposes a methodology for modeling anthropomorphism in human arm motion, and using this model for the inverse kinematics of a robot arm. Therefore, small errors in joint angle measurements do not affect the method's efficiency. A more accurate system for measuring arm motion could be used, without affecting the proposed method.

Since four subjects were used for recording arm motion, the variability of measurements across subjects was important. In Fig. 2, the histograms of each of the 5 modeled joint angles for the four subjects are shown. The histograms were constructed by using equal in number of samples experiments for each subject. As it can be seen, all subjects exhibited similar variability with respect to their arm motion in joint space. In the following section, the inter-joint variability across subjects is also analyzed.

2.2 Modeling Human Arm Movement

The modeling of human arm movement has received increased attention during the last decades, especially in the field of robotics [11] and graphics. This is because there is a great interest in modeling and understanding underlying laws and motion dependencies among the degrees of freedom of the arm, in order to incorporate them into robot control schemes. Most of the previous works in this area focus on the definition of motor primitives [12], or objective functions that are minimized during arm motion. These models lack the ability to describe dependencies among the degrees of freedom of the arm though. In this paper, in order to model the dependencies among the degrees of freedom of the arm during random 3D movements, graphical models were used.

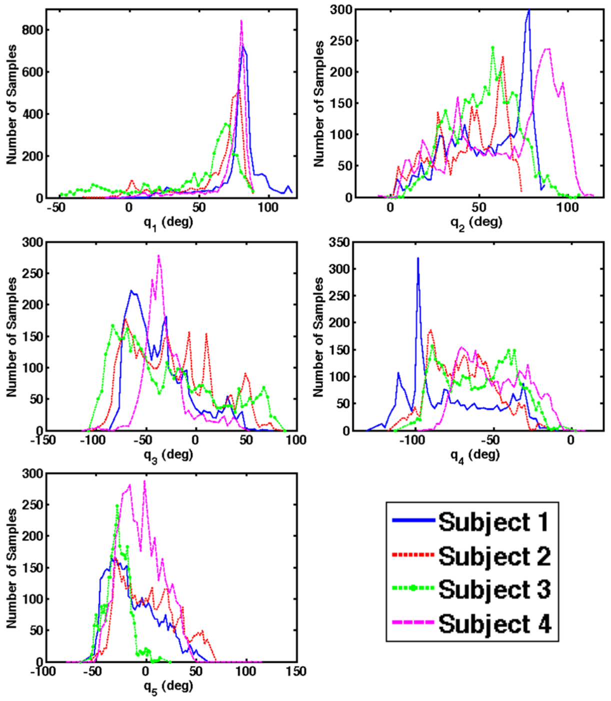

Fig. 2 Histograms of each joint angle across all subjects, for 4000 samples per subject.

2.2.1 Graphical Models

Graphical models are a combination of probability theory and graph theory [30]. They provide a tool for dealing with two characteristics; the uncertainty and the complexity of random variables. Given a set $\mathbf{F} = \left\{ f_1 \ldots f_N \right\}$ of random variables with joint probability distribution $p\left(f_1,\ \ldots,\ f_N\right)$, a graphical model attempts to capture the conditional dependency structure inherent in this distribution, essentially by expressing how the distribution factors as a product of *local functions*, (e.g. conditional probabilities) involving various subsets of $\mathbf{F}$. Directed graphical models, is a category of graphical models, also known as Bayesian Networks. A directed acyclic graph is a graphical model where there are no graph cycles when the edge directions are followed. Given a directed graph $G = (V, E)$, where V the set of vertices (or nodes) representing the variables $f_1,\ \ldots,\ f_N$, and E the set of directed edges between those vertices, the joint probability distribution can be written as follows:

$$p\left(f_1,\ \ldots,\ f_N\right) = \prod_{i=1}^{N} p\left(f_i \left| a\left(f_i\right)\right.\right) \tag{3}$$

[2] Deviation of the mean measured values for L_1 from the actual anatomical ones was 5%, 4%, 6%, 5% for the four subjects respectively. Likewise for L_2, it was 3%, 2%, 2%, 2%.

where, $a(f_i)$ the *parents* (or direct ancestors) of node f_i. If $a(f_i) = \emptyset$ (i.e. f_i has no parents), then $p(f_i | \emptyset) = p(f_i)$, and the node i is called the *root* node.

An advantage of graphical models is that the directed edges can be used to explicitly model causality. By inspecting the arrows in such models, it is easy to determine which variables directly influence others. Moreover, using (3) we can compute the joint probability for a set of variables to have a specific value, taking into account their dependencies learned from the training data. However, eq. (3) requires the parents of each variable, i.e. the structure of the graphical model. This can be learned from the training data, using the algorithm presented below.

2.2.2 Building the Model

A version of a directed graphical model is a tree model. Its restriction is that each node has only one parent. The optimal tree for a set of variables is given by the Chow-Liu algorithm [13]. Briefly, the algorithm constructs the maximum spanning tree of the complete mutual information graph, in which the vertices correspond to the variables of the model and the weight of each directed edge $f_i \to f_j$ is equal to the mutual information $I(f_i, f_j)$, given by

$$I(f_i, f_j) = \sum_{f_i, f_j} p(f_i, f_j) \log \frac{p(f_i, f_j)}{p(f_i)\, p(f_j)} \qquad (4)$$

where $p(f_i, f_j)$ the joint probability distribution function for f_i, f_j, and $p(f_i)$, $p(f_j)$ the marginal distribution probability functions for f_i, f_j respectively. Mutual information is a unit that measures the mutual dependence of two variables. The most common unit of measurement of mutual information is the bit, when logarithms to the base of 2 are used. It must be noted that the variables $\{ f_1 \ldots f_N \}$ are considered discrete in the definition of (4). Details about the algorithm of the maximum spanning tree construction can be found in [13].

Variables $\{q_1,\ q_2,\ q_3,\ q_4,\ q_5\}$ correspond to the joint angles of the 5 modeled degrees of freedom of the arm. They were rounded to the nearest integer, therefore, with a maximum rounding error of 0.5 deg, joint variables were essentially discretized enabling the simplification of the directed graphical model based training and inference algorithm without essential loss of information due to discretization. Using joint angle data recorded during the training phase from all the subjects, we could build the tree model. The resulting tree structure is shown in Fig. 3. Therefore, using (3), we defined the joint probability of the 5 variables representing joint angles by

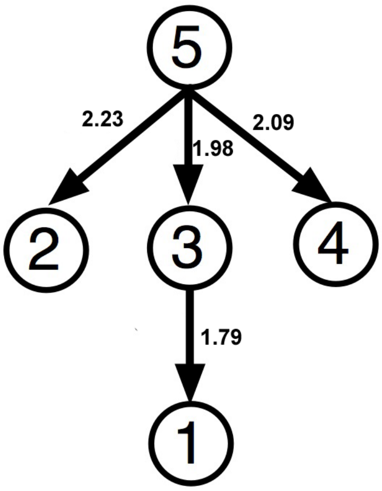

Fig. 3 The directed graphical model (tree) representing nodes (i.e. joint angles) dependencies. Node i corresponds to q_i. $i \to j$ means that node i is the parent of node j, where $i, j = 1, 2, 3, 4, 5$. The mutual information $I(i, j)$ is shown at each directed edge connecting i to j. The value of the mutual information quantifies the information gained if we describe two variables through their dependency, instead of considering them as independent. Its value is in bits.

$$p(q_1, q_2, q_3, q_4, q_5) = \prod_{i=1}^{5} p(q_i | a(q_i)) \qquad (5)$$

where $a(q_i)$ are the parents of variable q_i. Therefore, from the tree structure (see Fig. 3) it is

$$p(q_1, q_2, q_3, q_4, q_5) = p(q_1 | q_3)\, p(q_3 | q_5)\, p(q_4 | q_5)\, p(q_2 | q_5)\, p(q_5) \qquad (6)$$

where $p(q_i | q_j)$, $i, j = 1, 2, 3, 4, 5$, the conditional probability distribution of q_i, given its parent q_j. Each conditional probability was given by the following equation:

$$p(q_i | q_j) = \frac{p(q_i, q_j)}{p(q_j)} \qquad (7)$$

where $p(q_i, q_j)$ the joint probability distribution of q_i and its parent q_j and $p(q_j)$ the marginal probability distribution of q_j. A similar Bayesian framework for modeling human arm motion was also used by the authors in [14].

Eq (6) was essentially describing the dependencies between the joint angles, as identified by the graphical model. For each joint angle, this dependency could be described by the conditional probability distribution function with its parent, i.e. $p(q_i | q_j)$, $i, j = 1, 2, 3, 4, 5$. However, this function was based on the finite measurements during the human arm motion experiments, i.e. it was represented by a 2D histogram matrix. A way to conclude to a continuous representation of this function, was to fit this 2D histogram with a continuous function. This function was a Gaussian Mixture Model (GMM) [15]. A GMM is actually a weighted sum of Gaussian distribution functions, that can describe quite efficiently complex and non-smooth probability distribution functions. In general, for a N-dimensional GMM probability distribution function is given by:

$$p\left(\mathbf{Q}\right) = \sum_{k=1}^{h} \pi_k \mathcal{N}\left(\mathbf{M}_k, \mathbf{S}_k\right) \tag{8}$$

where h is the number of mixture components, while $\mathcal{N}\left(\mathbf{M}_k, \mathbf{S}_k\right)$ is a N-dimensional Gaussian distribution function with mean matrix $\mathbf{M}_k$ and covariance matrix $\mathbf{S}_k$ respectively. Details about the GMMs and their fitting procedure (Expectation Maximization (EM)) can be found in [15].

At this point it must be noted that the model presented previously was created using all the arm motion recorded from all the subjects. However, it would be of interest to show the inter-joint relationship for each subject separately. In other words, if a unique graphical model is trained to map anthropomorphism for each subject, it should be similar to the (global) model trained with data for all subjects, if the efficiency of the proposed method is to be assessed. For the latter to be proved, four different models were trained, each one using data from an individual subject. The models were proved to have the same structure as the global one shown in Fig. 3. This was due to the fact that similar inter-joint relationship were observed across all subjects. In order the latter to be quantified, a (5×5) mutual information matrix $\mathbf{I}_{\mathbf{m}}^{(n)}$ including all the mutual information indexes across the joint angles was computed for each subject n, $n = 1, 2, 3, 4$. Each (i, j) element of this matrix, $i, j = 1, \ldots 5$, is the mutual information index between the joint angles q_i and q_j, as computed by (4). This matrix was obviously symmetric, while the diagonal terms corresponded to the entropy of each joint angle. In Fig. 4 the mutual information matrices for each subject are graphically depicted. The patterns of the four matrices were very similar, which essentially proved that the inter-joint relationships were similar across subjects. Consequently, this observation proved that the method could capture robustly enough the global characteristics of anthropomorphism in human arm movements.

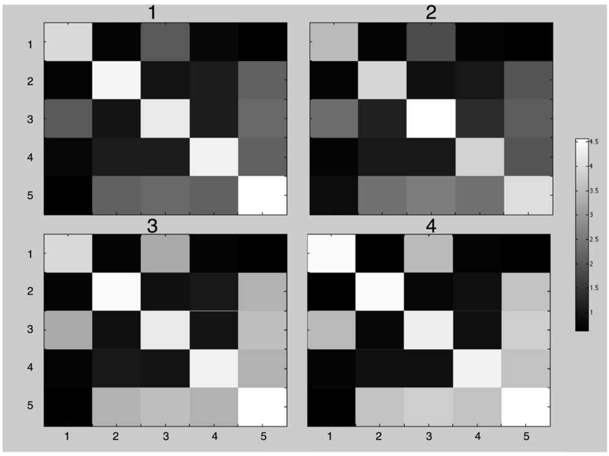

Fig. 4 Mutual information matrices for each of the four subjects. Same pattern of values was observed across subjects. Diagonal elements of matrices correspond to individual joint angle entropies, which are certainly higher than any mutual information index of two different joint angles. Values of elements $(5, 2)$, $(5, 3)$, $(5, 4)$, $(3, 1)$ (as well as their symmetric with respect to the diagonal elements) are higher than the other non-diagonal values, as expected from the structure of the model in Fig. 3.

2.3 Biomimetic Approach on Robot Inverse Kinematics

2.3.1 Inter-joint Dependencies

The graphical model shown in Fig. 3 along with (6) essentially described the dependencies among the joint angles of the human arm. These dependencies could be formulated as an objective function for a closed-loop robot inverse kinematic scheme, concluding to human-like robot configurations, since human multi-joint dependencies would have been taken into account.

For achieving the latter, we defined a function g_i for each of the joint angles q_i, $i = 1, 2, 3, 4, 5$, which was actually a probability density function (PDF) of a GMM, fitted on the data representing the conditional probability distribution function of the joint angle i given its parent joint angle j, $j = 1, 2, 3, 4, 5$. Therefore, using (7), the functions g_i for each joint angle q_i, $i = 1, 2, 3, 4, 5$, were defined as shown below:

$$\begin{aligned}
g_1 &= p\left(q_1 \left| q_3 \right.\right) = \frac{p(q_1, q_3)}{p(q_3)} = \frac{\sum_{k=1}^{n_{13}} \pi_k^{(1,3)} \mathcal{N}\left(\mathbf{M}_k^{(1,3)}, \mathbf{S}_k^{(1,3)}\right)}{\sum_{k=1}^{n_3} \pi_k^{(3)} \mathcal{N}\left(\mu_k^{(3)}, \sigma_k^{(3)}\right)} \\
g_2 &= p\left(q_2 \left| q_5 \right.\right) = \frac{p(q_2, q_5)}{p(q_5)} = \frac{\sum_{k=1}^{n_{25}} \pi_k^{(2,5)} \mathcal{N}\left(\mathbf{M}_k^{(2,5)}, \mathbf{S}_k^{(2,5)}\right)}{\sum_{k=1}^{n_5} \pi_k^{(5)} \mathcal{N}\left(\mu_k^{(5)}, \sigma_k^{(5)}\right)} \\
g_3 &= p\left(q_3 \left| q_5 \right.\right) = \frac{p(q_3, q_5)}{p(q_5)} = \frac{\sum_{k=1}^{n_{35}} \pi_k^{(3,5)} \mathcal{N}\left(\mathbf{M}_k^{(3,5)}, \mathbf{S}_k^{(3,5)}\right)}{\sum_{k=1}^{n_5} \pi_k^{(5)} \mathcal{N}\left(\mu_k^{(5)}, \sigma_k^{(5)}\right)} \\
g_4 &= p\left(q_4 \left| q_5 \right.\right) = \frac{p(q_4, q_5)}{p(q_5)} = \frac{\sum_{k=1}^{n_{45}} \pi_k^{(4,5)} \mathcal{N}\left(\mathbf{M}_k^{(4,5)}, \mathbf{S}_k^{(4,5)}\right)}{\sum_{k=1}^{n_5} \pi_k^{(5)} \mathcal{N}\left(\mu_k^{(5)}, \sigma_k^{(5)}\right)} \\
g_5 &= p\left(q_5\right) = \sum_{k=1}^{n_5} \pi_k^{(5)} \mathcal{N}\left(\mu_k^{(5)}, \sigma_k^{(5)}\right)
\end{aligned} \tag{9}$$

where $\pi_k^{(i,j)}$, $\mathbf{M}^{(i,j)}$, $\mathbf{S}^{(i,j)}$ were the components weights, mean and covariance matrices for the 2-dimensional Gaussian distributions fitted to joint distributions of

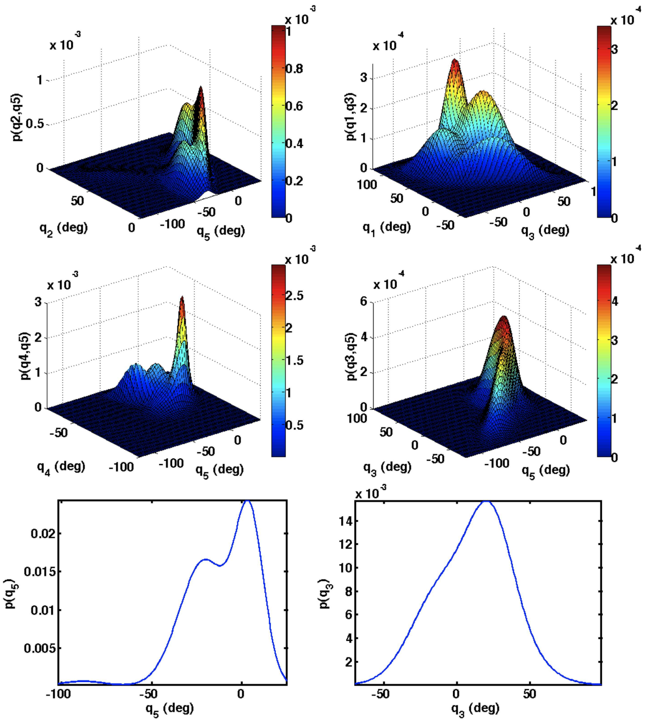

Fig. 5 Joint and marginal distribution functions after fitting the Gaussian Mixture Models. The non-uniform shape of the distributions justifies the choice of fitting them with GMMs.

Table 1 Number of mixing components used at the fitted GMMs.

	n_{13}	n_{25}	n_{35}	n_{45}	n_3	n_5
Number of components	4	4	6	6	3	3

joint angles q_i, q_j, and $\pi_k^{(i)}$, $\mu_k^{(i)}$, $\sigma^{(i)}$ were the components weights, mean and variance values for the 1-dimensional Gaussian distributions fitted to marginal distributions. n_{ij}, n_i were the numbers of the components used for fitting the GMMs to each distribution. Table 1 summarizes the number of mixture components used for each GMM. The number of the components was determined using the Akaike Criterion [16].

The g_i functions could take values from 0 to 1, since they were based on joint and marginal probabilities, while they were maximized if the corresponding joint coordination was frequently observed during the human arm motion. For example, g_1 was maximized towards a value for q_1 that was most frequently observed during human arm movements, for any given value for q_3. In this way, the g_i functions were maximized if the multi-joint configuration is anthropomorphic. This is also shown in Fig. 5, where the g_i functions are plotted for all the joint angles. The previously defined g_i functions were used in a closed-loop inverse kinematics scheme for solving the inverse kinematics of the robot arm.

2.3.2 Bio-mimetic closed-loop inverse kinematics

Since only the first 5 degrees of freedom of the robot arm were used, the robot joint angle vector was defined as:

$$\mathbf{q}_R = \left[q_{R_1} \; q_{R_2} \; q_{R_3} \; q_{R_4} \; q_{R_5} \right]^T \tag{10}$$

To solve the inverse kinematics problem, $\mathbf{q}_R$ must be computed starting from the (4×1) pose vector $\mathbf{p}_d = \left[x_d \; y_d \; z_d \; r_d \right]^T$, where x_d, y_d and z_d the desired 3D position of the robot end-effector, and r_d the desired roll orientation angle. Only these four variables can be controlled using the first 5 degrees of freedom of the robot arm, and therefore, the problem was still redundant [4]. An effective way to compute the inverse kinematics was that of resorting to the differential kinematics equation:

$$\dot{\mathbf{p}}_d = \mathbf{J}\left(\mathbf{q}_R\right) \dot{\mathbf{q}}_R \tag{11}$$

mapping the joint space velocity $\dot{\mathbf{q}}_R$ into the task space velocity $\dot{\mathbf{p}}_d$, where $\mathbf{J}\left(\mathbf{q}_R\right)$ is the (4×5) Jacobian matrix. This mapping may be inverted using the pseudo-inverse of the Jacobian matrix, i.e.,

$$\dot{\mathbf{q}}_R = \mathbf{J}^{\dagger}\left(\mathbf{q}_R\right) \dot{\mathbf{p}}_d \tag{12}$$

where $\mathbf{J}^{\dagger} = \mathbf{J}^T \left(\mathbf{J}\mathbf{J}^T\right)^{-1}$ is a (5×4) matrix, which corresponds to the minimization of the joint velocities in a least-squares sense [4]. Finally, the redundancy of the system can be further exploited using a task priority strategy corresponding to a solution of the inverse kinematics of the form:

$$\dot{\mathbf{q}}_R = \mathbf{J}^{\dagger}\left(\mathbf{q}_R\right) \dot{\mathbf{p}}_d + \left(\mathbf{I}_5 - \mathbf{J}^{\dagger}\left(\mathbf{q}_R\right) \mathbf{J}\left(\mathbf{q}_R\right)\right) \dot{\mathbf{q}}_a \tag{13}$$

where $\mathbf{I}_5$ is the (5×5) identity matrix, $\dot{\mathbf{q}}_a$ is an arbitrary joint velocity vector and the operator $\left(\mathbf{I}_5 - \mathbf{J}^{\dagger}\left(\mathbf{q}_R\right) \mathbf{J}\left(\mathbf{q}_R\right)\right)$ projects the joint velocity vector in the null space of the Jacobian matrix. This solution generates an internal motion of the robotic system (secondary task) which does not affect the motion of the robot arm end-effector (the primary task). The joint velocity vector $\dot{\mathbf{q}}_a$ can be used to move the robot joints in preferred regions, without affecting the robot end-effector position. In order to do that, the joint velocity vector $\dot{\mathbf{q}}_a$ can be chosen to be aligned with the gradient of an objective function $G\left(\mathbf{q}_R\right)$, i.e.:

$$\dot{\mathbf{q}}_a = k_a \frac{\partial G\left(\mathbf{q}_R\right)}{\partial \mathbf{q}_R} \tag{14}$$

with $k_a > 0$, in order to achieve a function optimization[3] for $G(\mathbf{q}_R)$. Finally the problem of inverse kinematics can be solved by defining (13) in a closed-loop form; given the desired pose vector $\mathbf{p}_d$, the joint space velocity $\dot{\mathbf{q}}_R$ can be computed by:

$$\dot{\mathbf{q}}_R = \mathbf{J}^{\dagger}(\mathbf{q}_R)\mathbf{K}\mathbf{e} + \left(\mathbf{I}_5 - \mathbf{J}^{\dagger}(\mathbf{q}_R)\mathbf{J}(\mathbf{q}_R)\right)\dot{\mathbf{q}}_a \qquad (15)$$

where

$$\mathbf{K} = \begin{bmatrix} k_1 & 0 & 0 & 0 \\ 0 & k_2 & 0 & 0 \\ 0 & 0 & k_3 & 0 \\ 0 & 0 & 0 & k_4 \end{bmatrix} \qquad (16)$$

where $k_1, k_2, k_3, k_4 > 0$ and $\mathbf{e}$ the position error vector, i.e. $\mathbf{e} = \mathbf{p}_d - \mathbf{p}$. The desired velocity of the end-effector is defined as zero, i.e. $\dot{\mathbf{p}}_d = 0$.

In order to incorporate the human-like robot configuration, we defined the objective function for each joint equal to the g_i function analyzed previously:

$$G(\mathbf{q}_R) = \left[g_1\ g_2\ g_3\ g_4\ g_5\right]^T \qquad (17)$$

In this way, the closed-loop inverse kinematics will tend to give solution that maximize the objective function $G(\mathbf{q})$, and consequently maximize g_i functions defined in (9). Due to the latter, the resulting robot arm configurations will be human-like, since the inverse kinematics will tend to result to robot configurations that describe the inter-joint dependencies learned from the human arm motions.

2.4 Generation of Anthropomorphic Arm Motions

Using the previously analyzed graphical model, we could also generate anthropomorphic arm motion. This was done by using inference algorithms for the graphical model, given a set of known variables of the model. In other words, since we were interested in generating motion, we could choose a value for the root joint angle (i.e. q_5), and then propagate through the structure of the tree and the conditional probabilities described by its edges, in order to calculate values for the other joint angles. This procedure is called *probabilistic inference* and is generally used in Bayesian Networks (like the graphical models) for the estimating the values of *hidden* nodes, given the values of the *observed* nodes [30].

In our case, we chose the root node (q_5) to be known (since we assigned a value for it), and through a message-passing algorithm, called *junction tree*, we could calculate the values for the other joint angles. For details on the inference algorithm, the reader should refer to [17]. It must be noted that the values of q_5 are not randomly chosen, but they are in the range of the values observed during training. In this way, we used the human inter-joint dependencies described by the graphical model in order to generate new motion for the robot arm. The generated anthropomorphic robot arm trajectories are analyzed in the Results section.

3 Results

3.1 Hardware and Experiment Design

The proposed architecture was assessed through the control of a redundant robot arm. The robot arm used was a 7 DoF anthropomorphic manipulator (PA-10, Mitsubishi Heavy Industries). The robot arm servo controller was interfaced with a PC through the ARCNET protocol, while the communication frequency was 500 Hz. The PC was senting desired joint velocity at each robot joint. Details on the modeling of the robot arm can be found in [18]. For building the model of the human arm movement, a magnetic position tracking system was used for recording human arm motion. The position tracking system (Isotrak II, Polhemus Inc.) was connected with a PC through serial communication interface (RS-232). The size of the position sensors was 2.83(W) 2.29(L) 1.51(H) cm.

For building the model of the human arm motion, the position tracker sensors were placed on the human arm, as shown in Fig. 1. The users were instructed to perform random 3D arm movements for about 5 minutes. Moreover, everyday life tasks were also performed, e.g. reaching and grasping objects on a table, or writing on a vertically positioned whiteboard. The position tracker measurements were collected and appropriately processed in order to construct the model describing human-like motion, analyzed previously. The processing of the data collected for 5 minutes lasted less than 2 minutes.

3.2 Robot Inverse Kinematics using the Biomimetic Approach

We first assessed the proposed method by controlling the end-effector position of the robot arm, using the previously analyzed approach for the inverse kinematics. The 3D position of the human hand[4], with respect to the shoulder, was recorded for 1 minute, while the user was performing random movements in the 3D space. Having the 3D position of the human hand, we assessed the proposed inverse kinematics approach by

[3] The robot should converge to anthropomorphic configurations that essentially (locally) maximize $G(\mathbf{q}_R)$.

[4] The human wrist point is actually analyzed here.

commanding the robot arm in joint space, in order to reach with its end-effector the same 3D point, with respect to its shoulder, i.e. the robot base. However, since the links of the human and robot arm had different length, the human hand 3D points should be appropriately transformed, in order for the robot arm to be able to reach them, with the same joint configuration. In other words, if the human arm reaches a point $\mathcal{P}$ in the 3D space with a configuration $\mathcal{Q}$, then a new (*equivalent*) point $\mathcal{P}'$ should be computed in order for the robot to reach it with the same configuration $\mathcal{Q}$.

3.2.1 Computation of Equivalent 3D Points

The computation of the equivalent points for the robot arm end-effector was based on the hypothesis that these would be the points where the human hand would reach, if the length of the human links (i.e. the upper arm and the forearm) would be equal to the respective robot links length. The hypothesis is illustrated in Fig. 6. For this reason, the position of the human elbow and wrist, already recorded using the position tracking system, were described using spherical coordinates, as shown in Fig. 6. If $\left[x_1\ y_1\ z_1\right]^T$, the Cartesian coordinates of the human elbow point, then its description in spherical coordinates was defined by:

$$\begin{bmatrix} r_1 \\ \varphi_1 \\ \theta_1 \end{bmatrix} = \begin{bmatrix} \sqrt{x_1^2+y_1^2+z_1^2} \\ atan2\left(y_1, x_1\right) \\ acos\left(\frac{z_1}{\sqrt{x_1^2+y_1^2+z_1^2}}\right) \end{bmatrix} \tag{18}$$

where r_1 was the radial (Euclidean) distance from the origin to the elbow, θ_1 was the inclination angle between the zenith direction and the line formed between the origin and the elbow point, while φ_1 was the azimuth angle between the reference direction on the chosen plane and the line from the origin to the projection of the elbow point on the plane. Virtually extending the upper arm to meet the length requirement of the robot arm, it would move the elbow point to a new position, that was described by Cartesian coordinates as follows:

$$\begin{aligned} x_1' &= R_1 \cos\varphi_1 \sin\theta_1 \\ y_1' &= R_1 \sin\varphi_1 \sin\theta_1 \\ z_1' &= R_1 \cos\theta_1 \end{aligned} \tag{19}$$

where R_1 was the length of the upper arm of the robot, as shown in Fig. 6. The human wrist point with respect to the human elbow point was described in spherical coordinates by:

$$\begin{bmatrix} r_2 \\ \varphi_2 \\ \theta_2 \end{bmatrix} = \begin{bmatrix} \sqrt{\left(x_2-x_1\right)^2+\left(y_2-y_1\right)^2+\left(z_2-z_1\right)^2} \\ atan2\left(y_2-y_1, x_2-x_1\right) \\ acos\left(\frac{z_2-z_1}{\sqrt{(x_2-x_1)^2+(y_2-y_1)^2+(z_2-z_1)^2}}\right) \end{bmatrix} \tag{20}$$

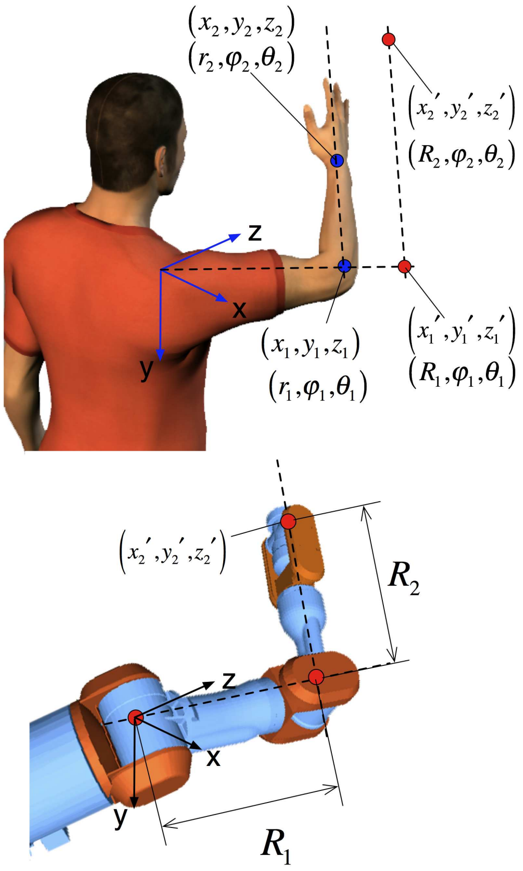
(x_2,y_2,z_2)
(r_2,φ_2,θ_2)
(x_2',y_2',z_2')
(R_2,φ_2,θ_2)
z
x
y
(x_1,y_1,z_1)
(r_1,φ_1,θ_1)
(x_1',y_1',z_1')
(R_1,φ_1,θ_1)
(x_2',y_2',z_2')
R_2
z
x
y
R_1

Fig. 6 Virtual elongation of the human upper arm and forearm to meet the robot links length requirements.

where r_2, θ_2 and φ_2 were defined similarly to r_1, θ_1 and φ_1 respectively and $\left[x_2\ y_2\ z_2\right]^T$ was the wrist position vector in Cartesian coordinates. Using the two orientation angles θ_2, φ_2 of the human forearm we could define the new wrist point for the robot arm, using as origin the new elbow point and the length requirements of the robot forearm. Finally, the Cartesian coordinates of the new wrist point, with respect to the base frame located at the shoulder, meeting the robot link length requirements, were given by:

$$\begin{aligned} x_2' &= R_2 \cos\varphi_2 \sin\theta_2 + x_1' \\ y_2' &= R_2 \sin\varphi_2 \sin\theta_2 + y_1' \\ z_2' &= R_2 \cos\theta_2 + z_1' \end{aligned} \tag{21}$$

where R_2 was the length of the robot forearm, as shown in Fig. 6. These new coordinates of the wrist point were used as desired position for the robot end-effector. The roll orientation angle of the human arm was not affected by the virtual extension of the human links.

3.2.2 Methodology Assessment

The biomimetic approach of the inverse kinematics proposed, was tested using the equivalent point of the wrist, i.e. $P'_2 = \left[x'_2 \; y'_2 \; z'_2\right]^T$, for the desired position of the robot end-effector. A continuous trajectory of the human hand was used and the resulted robot joint angle profiles were compared to the corresponding joint angle profiles of the human arm. Moreover, the method was also compared with the traditional closed-loop inverse kinematics method [4], which was defined by (15). However, since the robot was redundant, multiple solutions could be computed. For such robots, the most usual technique is to formulate the joint velocity vector $\dot{\mathbf{q}}_a$, such that the inverse kinematics converge to solutions that are away from the joint mechanical limits and also avoid singular configurations. The formulation of this problem is out of the scope of this paper and is analyzed in [4]. Therefore, our biomimetic approach was compared with the traditional closed-loop inverse kinematics formulated in a way to avoid joint limits and singular configurations. With this comparison, the effect of the proposed model that described the dependencies of the human arm movements on the robot inverse kinematics was illustrated.

In Fig. 7 the joint angle profiles of the human arm were compared to the robot joint angle profiles computed from the proposed inverse kinematics biomimetic approach and the traditional closed-loop inverse kinematics algorithm, for an arm movement of 12 sec. As it can be seen, the robot configuration using the proposed algorithm mimics the one of the human arm, while the traditional algorithm results to non-human like configurations. It must be noted that the proposed algorithm converged to the minimum error defined for the closed-loop inverse kinematics[5] in a comparable[6] number of loops to those needed by the the traditional algorithm. Snapshots of the human and robot configurations resulted from both algorithms, during this test, are shown in Fig. 8.

3.3 Generation of Anthropomorphic Robot Arm Motions

As mentioned in the section 2, the generation of anthropomorphic robot arm motions was based on the graphical model of multi-joint dependencies, and its ability to infer values for each node, given a starting value for at least one node. A continuous trajectory[7] for the root node (q_5) was commanded and the corresponding values for the other joint angles were computed through the inference algorithm of the model. Video snapshots of the robot arm performing the anthropomorphic trajectory are shown in Fig. 9, while the video of the robot arm movement is uploaded on the internet (see Fig. 9 caption). The resulted joint angle trajectories are shown in Fig. 10.

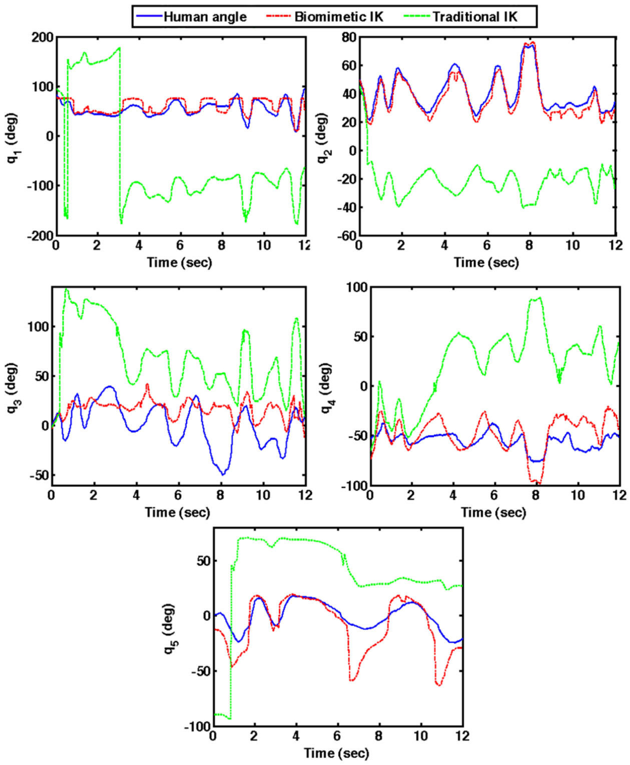

Fig. 7 Joint angles for the 5 robot joints as computed by the proposed method, compared to the corresponding human joint profiles and the profiles calculated by the traditional closed-loop inverse kinematics.

4 Conclusions and Discussion

A biomimetic approach in the inverse kinematics problem of redundant manipulators has been proposed. The resulted robot joint trajectories were based on a closed-loop inverse kinematic algorithm, augmented by a secondary factor that accounts for the biomimetic characteristic of the resulted robot arm configuration. This factor depends on a set of probability distributions that describe the correlations between the corresponding human joint angles. A graphical model was used to describe the human joint angle dependencies, by using training data collected offline from human arm movements in the 3D space. The proposed method was compared to a traditional closed-loop inverse kinematics scheme, and it was proved that by using the proposed

[5] A minimum error of 1 mm for each axis (x, y, z) and 1 deg for the roll angle was defined for both algorithms.

[6] An approximately 10% increase in the number of loops needed for convergence was noticed for the proposed algorithm, compared to the number of loops needed for the traditional inverse kinematics convergence.

[7] A ramp was chosen, that was appropriately designed to meet the probability distribution characteristics of this joint angle, as observed during training.

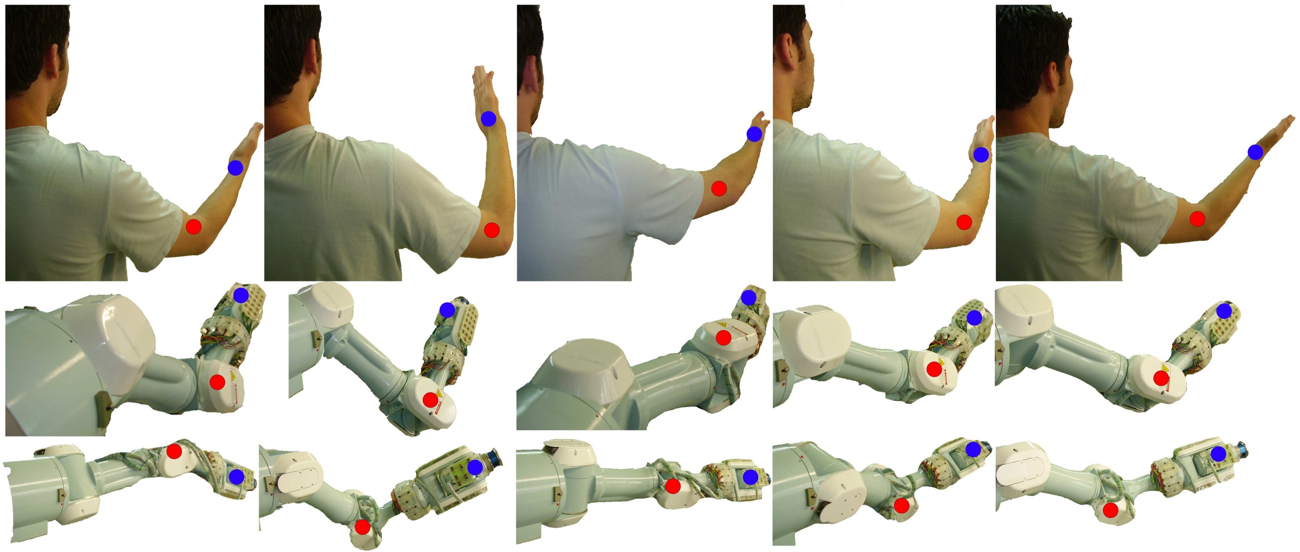

Fig. 8 Snapshots of the human arm performing random 3D motions and the robot arm driven by the proposed method and the traditional closed-loop inverse kinematics. 5 robot degrees of freedom are actuated. First line: The human performing random 3D arm motions. Second line: The robot arm driven by the proposed biomimetic inverse kinematics. Third line: The robot arm driven by the traditional inverse kinematics. Corresponding points are indicated with red and blue dots.

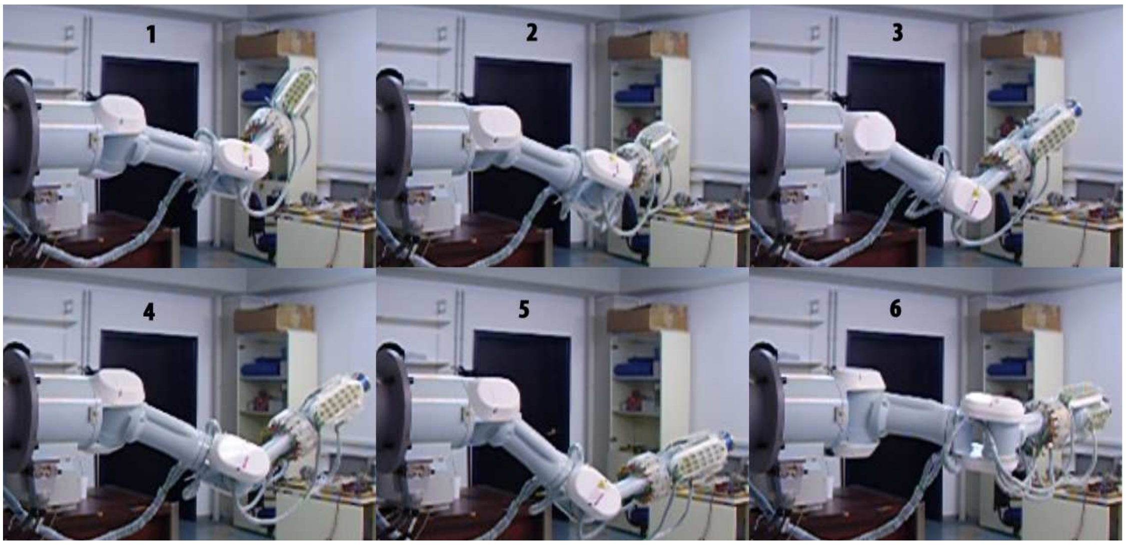

Fig. 9 Consecutive (1-6) snapshots of the generated anthropomorphic robot arm motion. 5 robot degrees of freedom are actuated. The video can be found in the Research section at the corresponding author's website (`http://web.mit.edu/partem/www`), or can be downloaded directly from the following link `http://web.mit.edu/partem/www/Site/Research_files/PA10_Biomimetic.MP4`

method, biomimetic robot arm motions are being produced. Moreover, the core of the biomimetic characteristic of the proposed method, i.e. the graphical model, was able to generate new anthropomorphic motions, not previously seen on training data.

The main novelty of the proposed method lies on two features; firstly, the method was not based on a finite set of human motion data, that should be reproduced by the robot arm, as described in previous works [7], [8]. Our method is not limited by the amount of training data and the resulting robot arm configurations are not restricted to identically mimic (i.e. copy) human arm configurations. Moreover the method is not based on optimizing algorithms and therefore there are no limitations due to computational cost. Indeed, it was shown that a closed-loop inverse kinematics scheme was able to converge slightly slower when it was augmented by the proposed method, than when it was used without it. The second novel feature of the proposed method is its ability to generate new motions. It was shown that anthropomorphic robot arm movements were generated by making use of the graphical model that describes human multi-joint coordination. Furthermore, the nature of the graphical model does not assume a specific robot arm kinematic structure, while the computations of the joint angles are not affected by the robot arm kinematics, as seen in previous works [10]. In other words, the method can be used with "non-human-arm like" robotic devices, if the appropriate correspondence between the human and robot joints is defined.

Most of the previous works in inverse kinematics for redundant manipulators focus on the minimization of objective function or task-defined criteria, as discussed above. This practice limits the number of possible solutions for the inverse kinematics, and in some cases, insufficient training data can significantly limit the range of application. In our work, the inverse kinematics solutions do not depend on the minimization of task-specific criteria, while the algorithm dependency on the training data is not explicit, allowing inverse kinematics to be solved, even if the specific task was never observed during training. In other words, the specific structure methodology allows for generalization, a feature that guarantees the existence of a solution to inverse kinematics. Finally, the proposed methodology can be used on learning a robot to move under a larger (or more specific) perspective. For example, using the proposed methodology a robot can be trained to move while handling hazardous materials, or in cluttered environments avoiding obstacles or specific configurations. Therefore, the proposed methodology can be used in a wide range of applications, in which a definition of an objective function for the solution of the inverse kinematics problem is not realizable. Using our method, a person can train, for example using a virtual reality environment, the robot to move in a specific manner, and then have the robot similarly perform the task in the real environment, which might be inaccessible or unknown for the user.

The value of the anthropomorphic robot motion can be assessed if a systematic survey on the new generation of robots is to be conducted. Anthropomorphic robot arm and hands, prosthetic or orthotic limbs, humanoid robots, service robots, surgical robots and much more, constitute a significantly growing area of advanced robots nowadays developed and used both for research reasons and every-day life applications. Therefore, and since robots are getting closer to humans, the necessity of *behaving* in an anthropomorphic way is getting larger. The authors strongly believe that anthropomorphism both in terms of design and control is a significant feature that robots should incorporate, in order to interact and help human every-day life in a safe and efficient perspective.

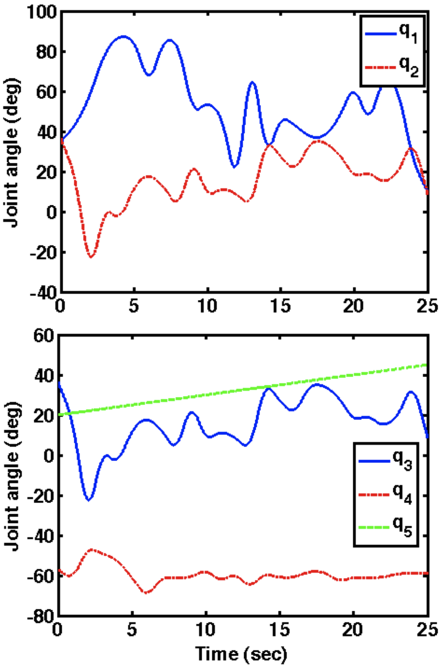

Fig. 10 Anthropomorphic robot joint angle profiles generated by the graphical model.

The proposed method can be useful in a wide range of robot arms that interface with human and are operated in human-cluttered environments. Especially in humanoid robots, the method can be directly used in order to result to anthropomorphic arm motions, while it can be easily extended to dual arm configurations, describing the joint angle dependencies in dual arm robotic systems. Future work will be devoted to add force capabilities and to extend the method to a robot arm-hand system.

A Human Arm Kinematics

As shown in Fig. 1, the arm is modeled as a 5 DoF mechanism, with 5 rotational joints, three at the shoulder and two at the elbow. The axes of joint 1, 2 and 3 are perpendicular to each other. Likewise, the axes of joints 4 and 5 are also perpendicular. The kinematics will be solved using the modified Denavit-Hartenberg (D-H) notation [19]. We assign frames at each rotational joint and then we can describe the relation between two consecutive frames $i-1$ and i by using the following homogeneous transformation matrix

$$T_i^{i-1} = \begin{bmatrix} c\theta_i & -s\theta_i & 0 & a_{i-1} \\ s\theta_i c\alpha_{i-1} & c\theta_i c\alpha_{i-1} & -s\alpha_{i-1} & -s\alpha_{i-1} d_i \\ s\theta_i s\alpha_{i-1} & c\theta_i s\alpha_{i-1} & c\alpha_{i-1} & c\alpha_{i-1} d_i \\ 0 & 0 & 0 & 1 \end{bmatrix} \tag{22}$$

where c, s correspond to cos and sin respectively, and θ, α, a and d the modified D-H parameters for the arm model given in Table 2, where L_1, L_2 the length of the upper arm and forearm respectively. Those lengths are calculated using the position tracker measurements as described in Methods section. The frames assignment, the base reference system placed on the shoulder, as

Table 2 Arm model modified D-H parameters

i	α_{i-1}	a_{i-1}	d_i	θ_i
1	0	0	0	q_1
2	$-90°$	0	0	q_2
3	$90°$	0	L_1	q_3
4	$-90°$	0	0	q_4
5	$90°$	0	L_2	q_5

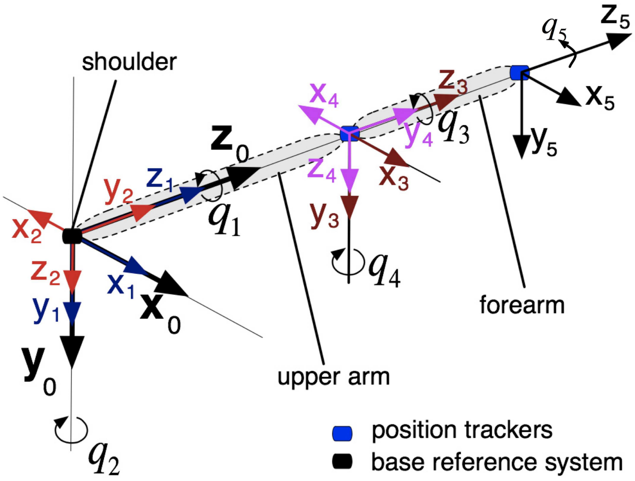

Fig. 11 Frames assignment, base reference system and position trackers along with modeled human joints.

well as the modeled joints and links are all shown in Fig. 11. Therefore, the transformation from the shoulder (frame 0) to the wrist (frame 5) is given by:

$$T_0^5 = T_0^1 T_1^2 T_2^3 T_3^4 T_4^5 \tag{23}$$

where the matrices T are defined according to (22). Measurements of the 3-dimensional (3D) position of the first position tracker provide the position of the frame 3, as shown in Fig. 11. The position and orientation of the frame 3 can be described by the following homogenous matrix:

$$T_0^3 = T_0^1 T_1^2 T_2^3 \tag{24}$$

where all matrices are defined through (22). The fourth column of the T_0^3 matrix is the 3D position of the frame 3, which coincides with the 3D position of the position tracker 1. Therefore, equating the fourth column of each side of (24) to the position vector of the position tracker, i.e. $\begin{bmatrix} x_1 & y_1 & z_1 & 1 \end{bmatrix}^T$, we get the q_1 and q_2 joint angles as described in the following equations:

$$q_1 = \arctan 2\,(\pm y_1, x_1) \tag{25}$$

$$q_2 = \arctan 2\left(\pm\sqrt{x_1^2 + y_1^2}, z_1\right) \tag{26}$$

Using (23) and using the fact that the position of the 2^{nd} position tracking sensor $\mathbf{T_2} = \begin{bmatrix} x_2 & y_2 & z_2 \end{bmatrix}^T$ coincides with the center of the 5^{th} frame, the matrix T_0^5 can be written as follows

$$T_0^5 = \begin{bmatrix} \mathbf{R}_{3x3} & \mathbf{T_2} \\ \mathbf{0}_{3x1} & 1 \end{bmatrix} \tag{27}$$

where $\mathbf{R}_{3x3}$ the rotation matrix describing the orientation of the 5^{th} frame and $\mathbf{0}_{3x1}$ a zero-element matrix with size 3 × 1. From (23) it is

$$\left(T_1^2\right)^{-1}\left(T_0^1\right)^{-1} T_0^5 = T_2^3 T_3^4 T_4^5 \tag{28}$$

Solving (28) by using (27) and equating the first 3 elements of the 4^{th} column of both sides, it is

$$x_2 c_1 c_2 + y_2 s_1 c_2 - z_2 s_2 = L_2 c_3 s_4 \tag{29}$$

$$x_2 c_1 s_2 + y_2 s_1 s_2 + z_2 c_2 = L_1 + L_2 c_4 \tag{30}$$

$$y_2 c_1 - x_2 s_1 = L_2 s_3 s_4 \tag{31}$$

where c_i, s_i correspond to $\cos(q_i)$, $\sin(q_i)$, $i = 1, 2, 3, 4$ respectively. From (29) and (31) it is

$$q_3 = \arctan 2\,(\pm B_3, B_1) \tag{32}$$

where

$$\begin{aligned} B_1 &= x_2 c_1 c_2 + y_2 s_1 c_2 - z_2 s_2 \\ B_3 &= y_2 c_1 - x_2 s_1 \end{aligned} \tag{33}$$

From (29), (30) it is

$$q_4 = \arctan 2\left(\pm\sqrt{B_1^2 + B_3^2}, B_2 - L_1\right) \tag{34}$$

where

$$B_2 = x_2 c_1 s_2 + y_2 s_1 s_2 + z_2 c_2 \tag{35}$$

Finally, since the reference system of the second position tracker is aligned with the frame 5, we can use one of the three orientation angles (i.e. the roll angle) in order to compute the joint angle q_5. The roll angle can be computed from (23) by the following equation:

$$\phi = a\tan 2\,(r_{32}, r_{33}) \tag{36}$$

where r_{32}, r_{33} are the (3,2) and (3,3) elements of the matrix $\mathbf{R}$ defined in (23) respectively, and ϕ the roll angle measured from the position tracker [4]. Solving (36) for q_5 using (23), it is:

$$q_5 = a\tan 2\,(\mathrm{M}, \Lambda) + a\tan 2\left(1 \pm \sqrt{\frac{\mathrm{K}^2}{\mathrm{M}^2 + \Lambda^2}}, \frac{\mathrm{K}}{\sqrt{\mathrm{M}^2 + \Lambda^2}}\right) \tag{37}$$

where

$$\begin{aligned} \mathrm{K} &= \tan(\phi)\,(c_2 c_4 - c_3 s_2 s_4) \\ \Lambda &= s_2 s_3 \\ \mathrm{M} &= c_3 c_4 s_2 + c_2 s_4 \end{aligned} \tag{38}$$

It must be noted that whenever more than one solutions for joint angles are provided from the above equations, one of them is finally selected, based on human joint limits and the definition of the joint angle directions.

Acknowledgements This work is partially supported by the European Commission through contract NEUROBOTICS (FP6-IST-001917) project and by the E.U.-European Social Fund (75%) and the Greek Ministry of Development-GSRT (25%) through the PENED project of GSRT.

References

1. A. A. Maciejewski & C. A. Klein, Obstacle Avoidance for Kinematically Redundant Manipulators in Dynamically Varying Environments, *The International Journal of Robotics Research*, 4, 109-117 (1985)
2. A. Ligeois, Automatic Supervisory Control of the Configuration and Behavior of Multibody Mechanism, *IEEE Transaction on Systems, Man and Cybernetics*, (1977)

3. Y. Nakamura & H. Hanafusa, Inverse Kinematics Solution with Singularity Robustness for Robot Manipulator Control, *ASME Journal of Mechanisms, Transmissions, Automation, Design*, 108, 163-171 (1986)
4. Lorenzo Sciavicco & Bruno Siciliano, Modeling and control of robot manipulators. McGraw-Hill (1996)
5. V. Potkonjak, M. Popovic, M. Lazarevic & J. Sinanovic, Redundancy problem in writing: From human to anthropomorphic robot arm, *IEEE Transaction on Systems, Man and Cybernetics, part B*, 28, 790-805, (1998)
6. V. Caggiano, A. De Santis, B. Siciliano & A. Chianese, A biomimetic approach to mobility distribution for a human-like redundant arm, *Proc. of the IEEE/RAS-EMBS International Conference on Biomedical Robotics and Biomechatronics*, 393-398, (2006)
7. N. S. Pollard, J. K. Hodgins, M. J. Riley & C. G. Atkeson, Adapting human motion for the control of a humanoid robot, *Proc. of IEEE Int. Conf. on Robotics and Automation*, 2, 1390-1397 (2002)
8. C. Kim, D. Kim & Y. Oh, Solving an inverse kinematics problem for a humanoid robots imitation of human motions using optimization, *Proc. of Int. Conf. on Informatics in Control, Automation and Robotics*, 85-92, (2005)
9. H. Cruse, E. Wischmeyer, M. Bruser, P. Brockfeld & A. Dress, On the cost functions for the control of the human arm movement, *Biological Cybernetics*, 62, 519-528, (1990)
10. T. Asfour & R. Dillmann, Human-like motion of a humanoid robot arm based on a closed-form solution of the inverse kinematics problem, *Proc. of IEEE/RSJ Int. Conf. on Intelligent Robots and Systems*, 2, 1407-1412, (2003)
11. A. Billard & M. J. Mataric, Learning human arm movements by imitation: Evaluation of a biologically inspired connectionist architecture, *Robotics and Autonomous Systems*, 37, 145-160, (2001)
12. A. Fod, M. J. Mataric & O. C. Jenkins, Automated derivation of primitives for movement classification, *Autonomous Robots*, 12, 39-54 (2002)
13. C. K. Chow & C. N. Liu, Approximating discrete probability distributions with dependence trees, *IEEE Transactions on Information Theory*, 14, 462-467 (1968)
14. Panagiotis K. Artemiadis & Kostas J. Kyriakopoulos, A Bio-inspired Filtering Framework for the EMG-based Control of Robots, *Proc. of 17th Mediterranean Conference on Control and Automation*, (2009)
15. G. McLachlan & D. Peel, Finite mixture models. John Wiley & Sons, Inc, (2000)
16. Hirotugu Akaike, A new look at the statistical model identification, *IEEE Transactions on Automatic Control*, 6, 716-723 (1974)
17. Yang Xiang, Probabilistic Reasoning in Multiagent Systems: A Graphical Models Approach. Inc. Gaithersburg, Maryland (2002)
18. N. A. Mpompos, P. K. Artemiadis, A. S. Oikonomopoulos & K. J. Kyriakopoulos, Modeling, full identification and control of the Mitsubishi PA-10 robot arm, *Proc. of IEEE/ASME International Conference on Advanced Intelligent Mechatronics*, (2007)
19. J. J. Craig, Introduction to robotics: mechanisms and control. Addison Wesley, MA (1989)
20. T. Flash & N. Hogan, The coordination of arm movements: an experimentally confirmed mathematical model,*J Neurosci*, 5, 1688-1703 (1985)
21. Y. Uno, M. Kawato & R. Suzuki, Formation and control of optimal trajectory in human multijoint arm movement, *Biological Cybernetics*, 61, 89-101 (1989)
22. A. G. Billard, S. Calinon & F. Guenter, Discriminative and adaptive imitation in uni-manual and bi-manual tasks, *Robotics and Autonomous Systems*, 54, 370-384 (2006)
23. T. Inamura, I. Toshima, H. Tanie & Y. Nakamura, Embodied symbol emergence based on mimesis theory, *International Journal of Robotics Research*, 24, 363-378 (2004)
24. A. Ijspeert, J. Nakanishi & S. Schaal, Movement imitation with nonlinear dynamical systems in humanoid robots, *Proceedings of International Conference on Robotics and Automation*, 1398-1403 (2004)
25. D. Bentivegna, C. Atkeson & G. Cheng, Learning tasks from observation and practice, *Robotics and Autonomous Systems*, 47, 163-169 (2004)
26. D. Kulic, W. Takano & Y. Nakamura, Incremental learning, clustering and hierarchy formation of whole body motion patterns using adaptive hidden markov chains, *International Journal of Robotics Research*, 27, 761-784 (2008)
27. L. Kovar, M. Gleicher & F. Pighin, Motion graphs, *ACM Transactions on Graphics*, 21, 473-482 (2002)
28. J. Lee, J. Chai, P. S. A. Reitsma, J. K. Hodgins & N. S. Pollard, Interactive Control of Avatars Animated With Human Motion Data, *ACM Transactions on Graphics*, 21, 491-500 (2002)
29. P. Pastor, H. Hoffmann, T. Asfour & S. Schaal, Learning and Generalization of Motor Skills by Learning from Demonstration, *Proceedings of the 2009 IEEE International Conference on Robotics and Automation*, (2009)
30. C. M. Bishop, Pattern Recognition and Machine Learning, Springer, (2006)